ACSNANO

www.acsnano.org

ARTICLE

Water-Induced Chiral Separation on a Au(111) Surface

Donglin Li,‡ Luye Sun,‡ Yuanqi Ding, Mengxi Liu, Lei Xie, Yinfu Liu, Lina Shang, Yangfan Wu, Hui-Jun Jiang, Lifeng Chi,* Xiaohui Qiu,* and Wei Xu*

Cite This: https://doi.org/10.1021/acsnano.1c07842

Read Online

ACCESS | Metrics & More | Article Recommendations | Supporting Information

ABSTRACT: Facing the scientific question of the origin of chirality in life, water is considered to play a crucial role in driving many biologically relevant processes *in vivo*. Water has been demonstrated *in vitro* to be related to chiral generation, amplification, and inversion, while the underlying mechanism is still not fully understood. Real-space evidence at the single-molecule level is thus urgently required to understand the role of water molecules in biomolecular chirality related issues. Herein, we choose one of the RNA bases, the biomolecule uracil (U), which self-assembles into racemic hydrogen-bonded structures. Upon water exposure, surprisingly, racemic structures could be transformed to homochiral water-involved structures, resulting in an unexpected chiral separation on the surface. The origin of chiral separation is due to preferential binding between water and the specific site of U molecules, which leads to the formation of the energetically most favorable homochiral $(U-H_2O-U)_2$ cluster as seed for subsequent chiral amplification. Such a water-driven self-assembly process may also be extended to other biologically relevant systems such as amino acids and sugars, which would provide general insights into the role that water molecules may play in the origin of homochirality *in vivo*.

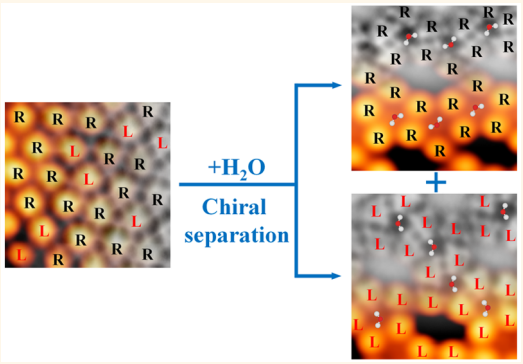

KEYWORDS: *water, chiral separation, chiral amplification, scanning tunneling microscopy, atomic force microscopy*

INTRODUCTION

Why does life require chirality? It is one of the most compelling puzzles and scientific questions today. Chirality is a universal phenomenon from single molecules to living organisms. Since the first example on the chiral separation of enantiomorphous crystals of sodium ammonium tartrate,[1] chirality has been recognized widely with great scientific interest in many fields such as biochemistry,[2−4] molecular biology,[5,6] pharmacology,[7−10] and material sciences.[11−14] It is well known that biomolecules in life such as sugars and amino acids are chiral and exist in only one enantiomer.[15−17] Water is one of the most important molecules *in vivo*,[18] which is demonstrated to play a crucial role in driving biological self-assembly processes,[19] while it is still unclear if the water molecule is related to the origin of chirality in life. Previously, water has been demonstrated to play a significant role *in vitro* in chiral generation,[20] chiral amplification,[21] chiral inversion,[22] *etc.* The underlying mechanism of water-induced chiral processes is still not fully understood. Thus, real-space evidence at the single-molecule level is urgently required to understand the corresponding physiochemical mechanism. An on-surface chemistry strategy allows to directly "see" molecular chirality-related issues by scanning tunneling microscopy (STM).[23−27] For example, homochiral pairs of cysteine molecules formed on Au(110) can be recognized.[28] In another case, a heterochiral heptahelicene dimer can be separated on Cu(111) by STM manipulation.[29] It is therefore of utmost interest and challenge to investigate the role of water molecules in molecular chiral origination, chiral amplification, and chiral separation in real space, with the aim of exploring the underlying mechanism, and more importantly, it may provide insights into the origin of chirality in life.

In this study, we choose one of the RNA bases, the biomolecule uracil (U), which self-assembles into a racemic disordered structure including various hydrogen-bonding configurations on the Au(111) surface (cf. Scheme 1), providing a model system to explore the role of water in perturbing hydrogen bonds and further influencing the racemic self-assembled U structure. Herein, using single-bond-resolved noncontact atomic force microscopy (nc-AFM) and STM

Received: September 7, 2021
Accepted: October 11, 2021

Scheme 1. Schematic illustration of the water-induced chiral separation from both racemic disordered and ordered U self-assembled structures to homochiral ordered U+H_2O structure. The racemic disordered U self-assembled structure can be transformed to the racemic ordered one by annealing at 330 K, whereas this phase transition can be achieved by desorption of water molecules from a U+H_2O structure at room temperature. The hydrogen bonds are depicted by blue dashed lines. R and L notations denote the chiralities of individual molecules. Structural model: H: white, C: gray, N: blue, O: red

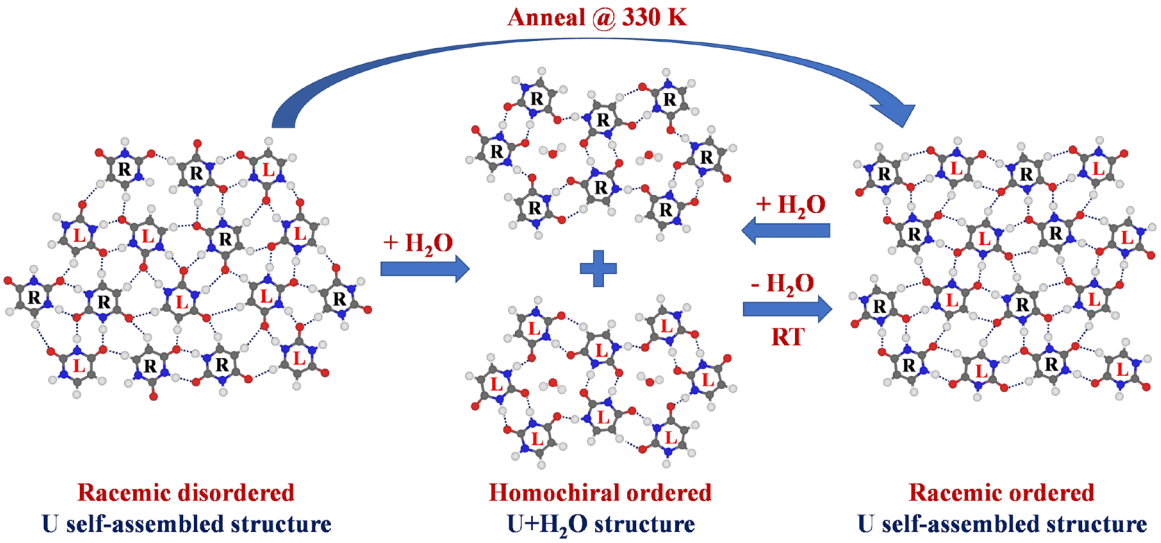

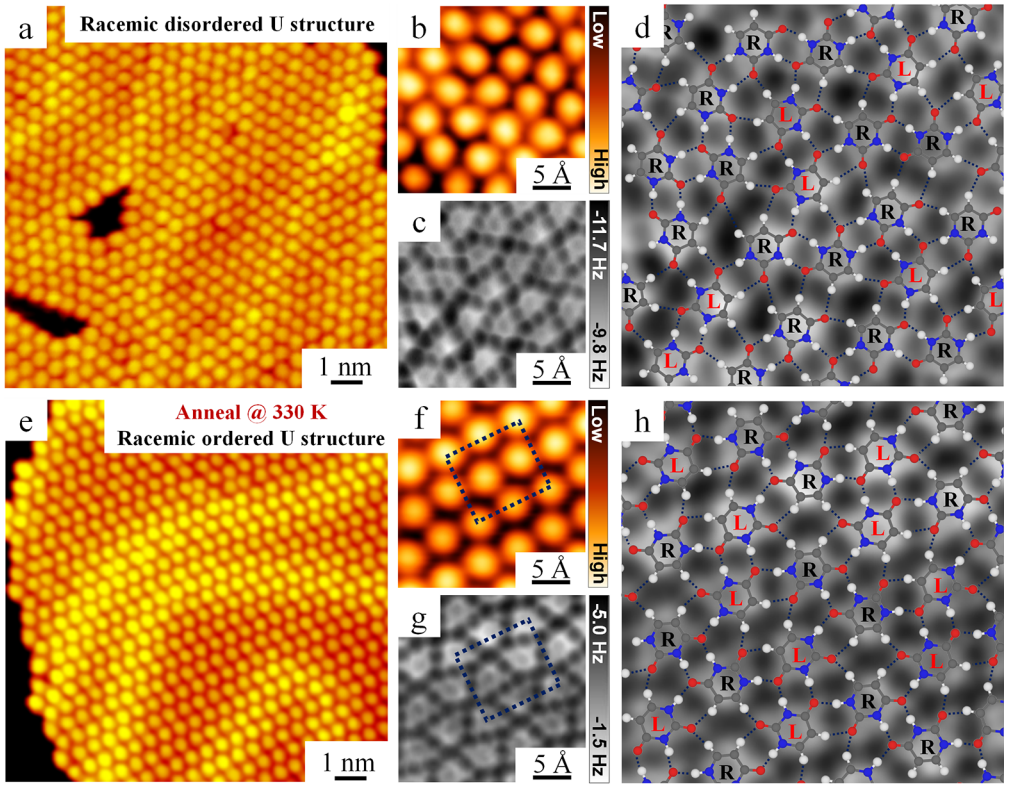

Figure 1. Amorphous-to-crystalline phase transformation of U self-assembled structures by annealing at 330 K on Au(111). (a) STM image of a close-packed disordered U self-assembled structure. (b, c) High-resolution STM image and the corresponding single-bond-resolved nc-AFM image of the disordered U structure, respectively. (d) Enlarged nc-AFM image of (c) with the calculated model superimposed showing the disorderliness of this racemic structure. (e) STM image of a close-packed ordered U self-assembled structure after annealing the disordered one at 330 K. (f, g) High-resolution STM image and the corresponding nc-AFM image of the ordered U structure with the depicted unit cells, respectively. (h) Enlarged nc-AFM image of (g) with the calculated model superimposed showing the orderliness of this racemic structure. The hydrogen bonds are depicted by blue dashed lines. R and L notations denote the chiralities of individual molecules. Structural model: H: white, C: gray, N: blue, O: red.

imaging, which allows direct identification of the chirality of prochiral U molecules adsorbed on the surface, we demonstrate that after depositing water molecules, surprisingly, the racemic disordered U self-assembled structure is trans-

https://doi.org/10.1021/acsnano.1c07842
ACS Nano XXXX, XXX, XXX−XXX

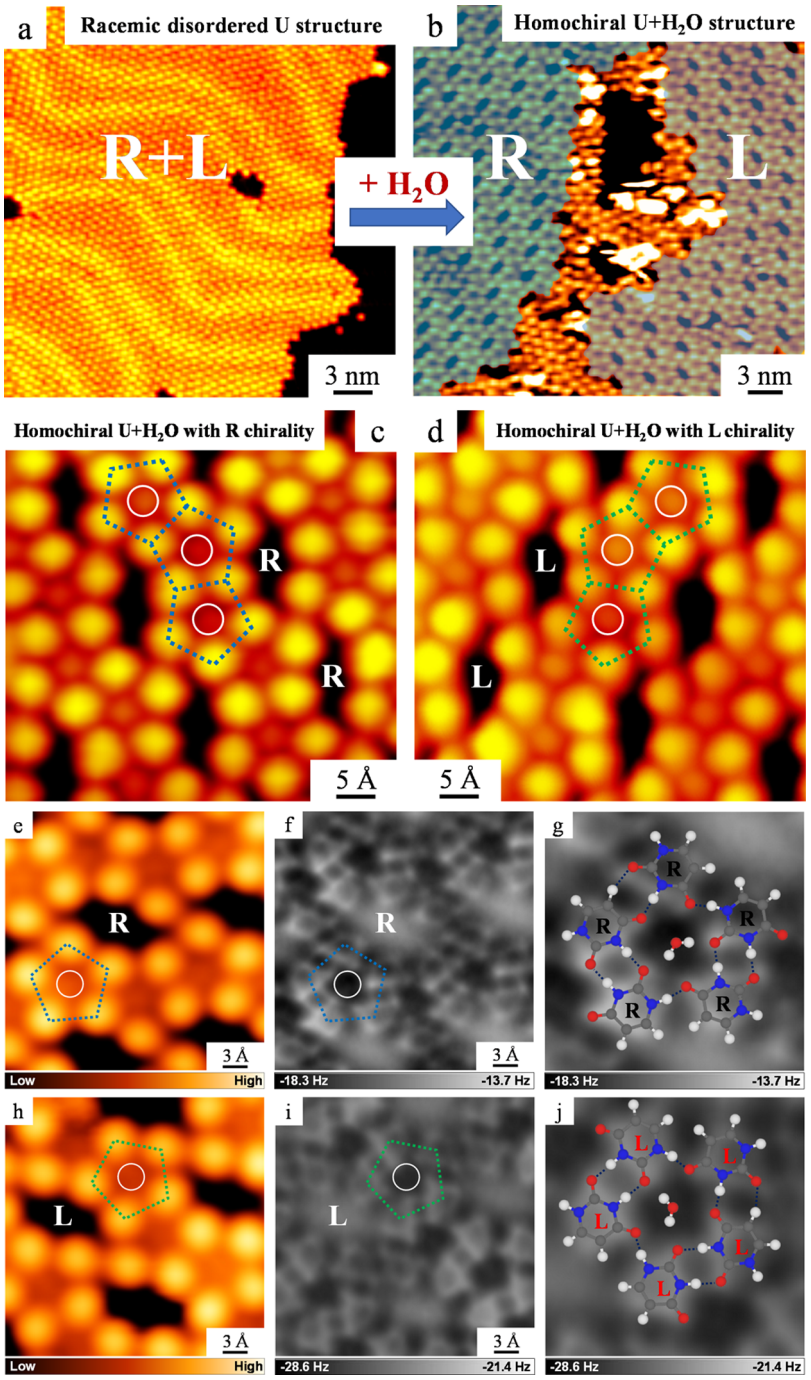

Figure 2. Experimental process of water-induced chiral separation from a racemic disordered U structure to a homochiral ordered U+H_2O structure. (a) STM image of the racemic disordered U self-assembled structure. (b) Larger-scale STM image showing the coexistence of homochiral U+H_2O structures with R and L chiralities. (c, d) STM images of a 2D homochiral U+H_2O structure with R and L chirality, respectively, which could be distinguished from the cavities as indicated by R and L. (e, f) High-resolution STM image and the corresponding nc-AFM image of the U+H_2O structure with R chirality, respectively. (g) Enlarged nc-AFM image of a five-membered ring with the calculated model superimposed. (h, i) High-resolution STM image and the corresponding nc-AFM image of the U+H_2O structure with L chirality, respectively. (j) Enlarged nc-AFM image of a five-membered ring with the calculated model superimposed. The hydrogen bonds are depicted by blue dashed lines. Structural model: H: white, C: gray, N: blue, O: red.

formed to a homochiral water-induced ordered U+H_2O structure, which results in an unexpected chiral separation process on the surface. The racemic disordered U structure can be transformed to a racemic ordered one by annealing the substrate at 330 K, leading to an amorphous-to-crystalline phase transition. Moreover, interestingly, such a water-induced chiral separation can also be achieved by phase transition from the racemic ordered U structure to the homochiral U+H_2O structure. Desorption of water molecules from the homochiral U+H_2O structure leads to formation of the racemic ordered U structure (cf. Scheme 1). The origin of chiral separation is investigated in detail by extensive DFT calculations, and the key is that formation of the elementary homochiral (U−H_2O−U)$_2$ cluster is energetically more favorable than any other

https://doi.org/10.1021/acsnano.1c07842
ACS Nano XXXX, XXX, XXX−XXX

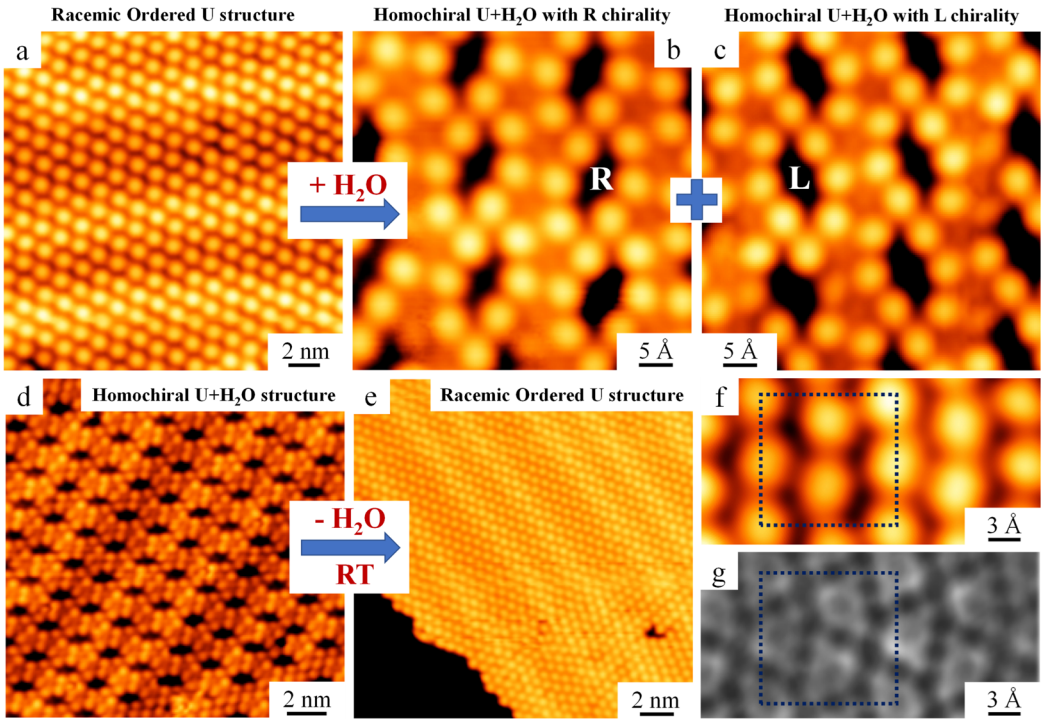

Figure 3. Reversible experimental process from the racemic ordered U structure to the homochiral U+H_2O structure and back to the racemic ordered U structure. (a–c) STM images showing the phase transformation from the racemic ordered U self-assembled structure to the homochiral U+H_2O structure achieving water-induced chiral separation. (d, e) STM images showing the reversed process from the U+H_2O structure to the ordered U structure by desorption of water molecules at RT. (f, g) High-resolution STM image and the corresponding nc-AFM image of the ordered U structure with the depicted unit cells, respectively.

proposed heterochiral $(U–H_2O–U)_2$ clusters. Subsequently, *via* three chiral amplifications, the homochiral $(U–H_2O–U)_2$ clusters grow into homochiral $(U–H_2O–U)_2$ chains further to homochiral U+H_2O five-membered ring chains, and finally to a homochiral 2D U+H_2O structure. These findings provide real-space evidence of specific hydrogen-bonding interactions between water and U molecules, which is the main driving force for chiral separation from racemic molecular self-assembled structures to water-involved homochiral ones, which also provides insights into the role that water molecules may play in the origin of homochirality *in vivo*.

RESULTS AND DISCUSSION

As shown in Figure 1a, a close-packed self-assembled structure is formed after depositing the U molecules on the Au(111) surface. The high-resolution STM image and the corresponding nc-AFM image of this structure are shown in Figure 1b and c, respectively. For direct identification of the chirality of U molecules in the nc-AFM images, the chemical structure of the U molecule, which is defined as R chirality, and the corresponding simulated AFM image are shown in Figure S1a and Figure S1b, respectively. Figure S1c shows the simulated AFM image with a structural model superimposed, showing that the C═C bond, which presents a pronounced contrast in the simulated AFM image, is used to identify the chirality of U molecules. In order to analyze such a structure in detail, we then propose the structural model relaxed by the DFT method, which is overlaid on the enlarged nc-AFM image (Figure 1d). Interestingly, from the model, we identify that such a close-packed structure is actually a racemic disordered hydrogen-bonded structure. Furthermore, after annealing the disordered structure at 330 K, we observe the formation of a seemingly ordered close-packed structure as shown in Figure 1e. We then also superimpose the DFT-relaxed model on the enlarged nc-AFM image (Figure 1h) and distinguish that such a close-packed structure is indeed an ordered one with both R and L chiralities. The unit cell of the structure indicated by a blue contour is depicted in the high-resolution STM image (Figure 1f) and the corresponding nc-AFM image (Figure 1g), respectively.

In the next step, we introduce water molecules at a pressure of $\sim 8 \times 10^{-5}$ mbar into an ultra-high-vacuum (UHV) system. After deposition of water molecules on the racemic disordered U self-assembled structure (shown in Figure 2a) at RT, surprisingly, we observe a structural transformation from the close-packed one to a more opened one (shown in Figure 2b) with R and L chiralities coexisting. A closer inspection (Figure 2c and d) allows us to identify that such a U+H_2O structure is composed of characteristic alternating five-membered ring motifs depicted by blue and green pentagon contours, respectively. The dot protrusion within each five-membered ring is assigned to a water molecule, as depicted by a white circle. To further reveal the atomic-scale details of the U+H_2O structure (Figure 2e), we obtain the nc-AFM image with single-bond resolution (Figure 2f). Figure 2g shows the enlarged nc-AFM image of a five-membered-ring motif (highlighted in Figure 2e and f) superimposed with the calculated structural model, which allows to identify the motif is composed of homochiral U molecules (with R chirality in this structure) and a water molecule forming intermolecular hydrogen bonds. The corresponding U+H_2O structure with another chirality is demonstrated in Figure 2h–j. Based on the above analysis, it is demonstrated that water-induced chiral separation is achieved by structural transformation from the

https://doi.org/10.1021/acsnano.1c07842
ACS Nano XXXX, XXX, XXX–XXX

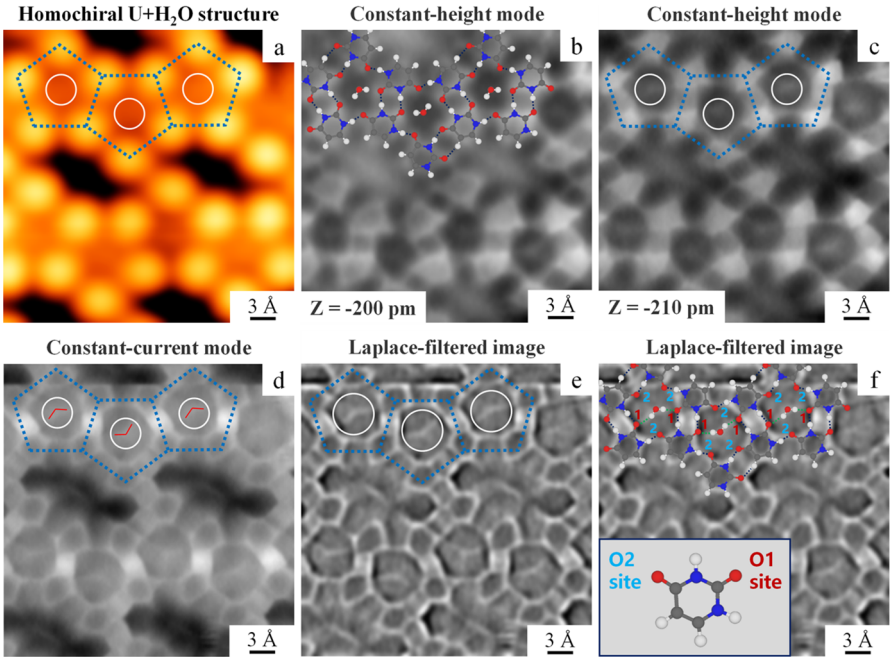

Figure 4. Real-space experimental evidence to identify the interaction between water molecules and U molecules. (a–c) High-resolution STM image and the corresponding constant-height nc-AFM images at different tip distances (z = −200 pm and −210 pm) of the U+H_2O structure. The alternating five-membered-ring motifs and the calculated model are depicted by blue pentagon contours and superimposed on the corresponding images, respectively. (d, e) nc-AFM images in constant-current mode (V = −10 mV, I = 50 pA) and the corresponding Laplace-filtered images present more hints to identify the hydrogen-bonding configurations between water and U molecules. (f) The calculated model of U+H_2O structure is superimposed on the Laplace-filtered nc-AFM image where the water-involved hydrogen bonds are depicted by green dashed lines. The O atom between two imines of U molecule is assigned to the O1 site, and the other O atom is assigned to the O2 site, as shown in the inset.

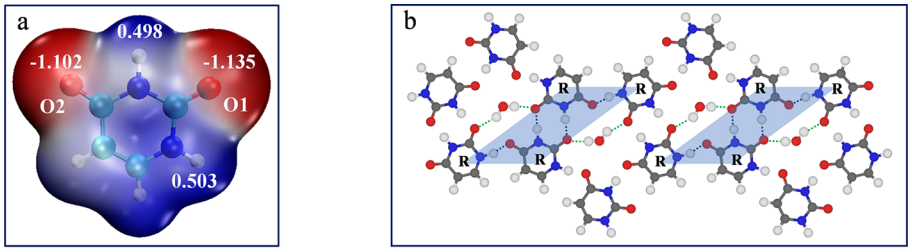

c

The origin of chiral separation

(U-H_2O-U)$_2$ clusters	Optimized model of observed structure	Optimized models of proposed structures		
	Homochiral (U-H_2O-U)$_2$ cluster	Heterochiral (U-H_2O-U)$_2$ cluster	Heterochiral (U-H_2O-U)$_2$ cluster	Heterochiral (U-H_2O-U)$_2$ cluster
	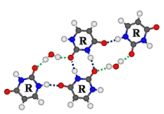	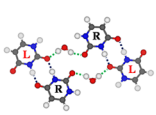	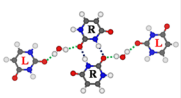	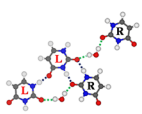
Total energy (eV)	0 eV	0.155 eV	0.908 eV	2.335 eV

Figure 5. DFT-optimized models and the corresponding total energies of different structural motifs. (a) The electrostatic potential map qualitatively shows the negatively charged oxygen atoms and positively charged hydrogen atoms of the U molecule (red and blue colors represent negative and positive potential regions, respectively). Bader charge analysis with numbers indicated (substrate is omitted for clarity). (b) The most relevant homochiral (U–H_2O–U)$_2$ cluster as the elementary structural motif (highlighted by a blue parallelogram) of the homochiral U+H_2O structure. (c) DFT calculations on a series of (U–H_2O–U)$_2$ clusters are performed on Au(111) (the substrate is omitted for clarity). The total energies of these optimized structures are shown below.

https://doi.org/10.1021/acsnano.1c07842
ACS Nano XXXX, XXX, XXX–XXX

racemic disordered U structure to the homochiral ordered U +H_2O structure.

To demonstrate the generality of such a water-induced chiral separation process, deposition of water molecules on the racemic ordered U self-assembled structure (shown in Figure 3a) has been performed. Interestingly, upon water exposure, phase transformation from the racemic ordered U structure to the homochiral U+H_2O structures (shown in Figure 3b and c) also occurs, thus indicating water-induced chiral separation is achieved as well. Moreover, we perform further experiments by desorption of water molecules from the homochiral U+H_2O structure. Intriguingly, we put U+H_2O structures at RT for 90 min, and it is found that the U+H_2O structure is transformed back to the close-packed one as shown in Figure 3d and e. From the high-resolution STM image and the corresponding nc-AFM image shown in Figure 3f and g, we further identify that the close-packed structure is actually the racemic ordered U structure and the unit cell is depicted by blue contours as shown in Figure 3f and g, respectively. Therefore, we achieve a reversible conversion between the racemic ordered U structure and the homochiral U+H_2O structures.

In order to determine the atomic-scale details of hydrogen-bonding configurations between water and U molecules. We resort to single-bond-resolved nc-AFM imaging again. As shown in Figure 4a−c, from the STM image and the corresponding nc-AFM images in constant-height mode at different tip distances, it is distinguished that the water molecule (depicted by a white circle) is imaged as a dot protrusion from STM imaging and shows a more pronounced hydrogen-bonding configuration with U molecules from nc-AFM imaging. Especially, to get more conformational information,[30] constant-current-mode nc-AFM imaging is applied, as shown in Figure 4d, where the water-involved hydrogen-bonding configurations can be clearly recognized, as indicated by red bent lines, which is more unambiguously distinguished in the corresponding Laplace-filtered image (Figure 4e). Together with the constant-height mode image (Figure 4b) where the U molecular configurations can be clearly identified, we then propose and calculate the model of alternating five-membered-ring motifs that are superimposed on the Laplace-filtered image (Figure 4f), in which the water-involved hydrogen bonds are specifically depicted, and more importantly, it is found that water molecules preferentially bind to O1 sites of U molecules (*cf.* the inset).

Such a preferential binding between a water molecule and O1 sites of U molecules within the five-membered-ring motif is theoretically explained as shown in Figure 5a, in which Bader charge analysis quantitatively shows that the O1 site is more negatively charged than the O2 site. Then the key question is if such a preferential binding between water and U molecules is related to the origin of chiral separation. To explore the driving force of water-induced chiral separation, we further analyze the homochiral U+H_2O structure and extract the most relevant homochiral $(U-H_2O-U)_2$ cluster as the elementary structural motif, as highlighted by a blue parallelogram in Figure 5b. We then perform extensive DFT calculations on a series of structures on Au(111). As shown in Figure 5c, four different $(U-H_2O-U)_2$ clusters are calculated, in which the homochiral $(U-H_2O-U)_2$ cluster is the one observed experimentally, and the other three heterochiral $(U-H_2O-U)_2$ clusters are built up based on the preferential binding sites between water and U molecules. After relaxation, it is found that the homochiral $(U-H_2O-U)_2$ cluster is the most stable one, indicating the formation of the homochiral $(U-H_2O-U)_2$ cluster *via* preferential binding between water and U molecules is consequently the origin of chiral separation.

From the above analysis, the whole scenario of water-induced chiral separation and subsequent formation of a homochiral 2D U+H_2O structure are presented as follows: (i) Upon water exposure, all of hydrogen bonds between U molecules within both the racemic disordered and the racemic ordered U structures are broken (*cf.* Table S1 for extensive calculations on different hydrogen-bonded dimer configurations extracted from self-assembled U structures), and then water molecules preferentially bind the O1 sites of U molecules to form the elementary homochiral $(U-H_2O-U)_2$ cluster (Figure S2a). (ii) Based on the available binding sites of the homochiral $(U-H_2O-U)_2$ cluster, R−R interconnection between $(U-H_2O-U)_2$ clusters *via* dimer 4 (*cf.* Table S1) is energetically more favorable than the possible R−L interconnections *via* dimer 7 or dimer 9 (*cf.* Table S1), which results in the formation of a homochiral $(U-H_2O-U)_2$ chain (Figure S2b) achieving the first step of chiral amplification. (iii) In the next step, individual U molecules with the same chirality are hydrogen-bonded to the $(U-H_2O-U)_2$ chain (*via* dimer 8) on both sides to close the ring, which leads to formation of a homochiral U+H_2O five-membered-ring chain (Figure S2c), achieving the second chiral amplification. (iv) In the last step, homochiral U+H_2O five-membered-ring chains are hydrogen-bonded together *via* the same chirality (*via* the most stable dimer 1) into the homochiral 2D U+H_2O structure (Figure S2d), achieving the third chiral amplification.

CONCLUSION

In conclusion, from a combination of high-resolution STM and nc-AFM imaging, we investigate the interactions between water and a biologically relevant molecule U, *i.e.*, a water-driven self-assembly process, and demonstrate in real space that an unexpected water-induced chiral separation occurs on the surface. The origin of chiral separation is due to the preferential binding between water and the specific site of U molecules. Such a water-driven self-assembly process may also be extended to other biologically relevant systems such as amino acids and sugars, which would provide general insights into the role that water molecules may play in the origin of homochirality *in vivo*.

METHODS

STM/nc-AFM Measurements. All experiments were carried out in three commercial UHV systems (Createc LT-STM, SPECS variable-temperature "Aarhus-type" STM[31,32] and Scienta Omicron LT-STM/AFM) at a base pressure better than ~3×10^{-10} mbar. The Au(111) surface was prepared by several cycles of argon ion sputtering followed by annealing at 800 K for 10 min. We purchased the uracil molecules (purity higher than 98%) and pure deionized water from Sigma-Aldrich. The deionized water was purified by several freeze−thaw cycles.[33] We deposited uracil and water molecules by thermal sublimation and through a leak valve, respectively. Scanning conditions of the SPECS variable-temperature STM: I_t = 0.5−0.9 nA, V_t = −1700 mV. For the experiments performed in the Scienta Omicron system, the voltage was applied on the tip while the sample was grounded. The STM images were taken in the constant-current mode, and the nc-AFM measurement was carried out with a CO-functionalized tip (quality factor $Q = 8 \times 10^4$, oscillation amplitude A = 100 pm, resonance frequency f_0 = 39.65 kHz) both in constant-height and constant-current mode at liquid helium temperature.

https://doi.org/10.1021/acsnano.1c07842
ACS Nano XXXX, XXX, XXX−XXX

Theoretical Calculations. The Vienna *ab initio* simulation package (VASP)[34,35] was used to perform the DFT calculations by using the Perdew–Burke–Ernzerhof generalized gradient approximation (GGA) exchange–correlation functional.[36] For describing the interaction between electrons and ions, the projector-augmented wave method was used.[37,38] The dispersion-corrected DFT-D3 method[39] was used to consider the van der Waals interactions. The atomic structures were relaxed until the atomic forces were less than 0.03 eV/Å. The electrostatic potential map was calculated with B3LYP/6-31G** (Gaussian 09) combined with Multiwfn 3.7.[40,41] The model provided by Hapala *et al.* was used to simulate the AFM images with a flexible CO tip (k_{tip} = 0.5 N m^{-1}).[42]

ASSOCIATED CONTENT

Supporting Information

The Supporting Information is available free of charge at https://pubs.acs.org/doi/10.1021/acsnano.1c07842.

Figures of simulated AFM image, additional DFT calculations on various hydrogen-bonded U dimers, and a scheme showing the process of chiral separation and amplification (PDF)

AUTHOR INFORMATION

Corresponding Authors

Lifeng Chi − *Institute of Functional Nano & Soft Materials (FUNSOM), Jiangsu Key Laboratory for Carbon-Based Functional Materials and Devices, Joint International Research Laboratory of Carbon-Based Functional Materials and Devices, Soochow University, Suzhou 215123, People's Republic of China;* orcid.org/0000-0003-3835-2776; Email: chilf@suda.edu.cn

Xiaohui Qiu − *CAS Key Laboratory of Standardization and Measurement for Nanotechnology, CAS Center for Excellence in Nanoscience, National Center for Nanoscience and Technology, Beijing 100190, People's Republic of China; University of Chinese Academy of Sciences, Beijing 100049, People's Republic of China*; Email: xhqiu@nanoctr.cn

Wei Xu − *Interdisciplinary Materials Research Center, College of Materials Science and Engineering, Tongji University, Shanghai 201804, People's Republic of China;* orcid.org/0000-0003-0216-794X; Email: xuwei@tongji.edu.cn

Authors

Donglin Li − *Interdisciplinary Materials Research Center, College of Materials Science and Engineering, Tongji University, Shanghai 201804, People's Republic of China*

Luye Sun − *CAS Key Laboratory of Standardization and Measurement for Nanotechnology, CAS Center for Excellence in Nanoscience, National Center for Nanoscience and Technology, Beijing 100190, People's Republic of China; University of Chinese Academy of Sciences, Beijing 100049, People's Republic of China*

Yuanqi Ding − *Interdisciplinary Materials Research Center, College of Materials Science and Engineering, Tongji University, Shanghai 201804, People's Republic of China*

Mengxi Liu − *CAS Key Laboratory of Standardization and Measurement for Nanotechnology, CAS Center for Excellence in Nanoscience, National Center for Nanoscience and Technology, Beijing 100190, People's Republic of China; University of Chinese Academy of Sciences, Beijing 100049, People's Republic of China;* orcid.org/0000-0001-7009-5269

Lei Xie − *Interdisciplinary Materials Research Center, College of Materials Science and Engineering, Tongji University, Shanghai 201804, People's Republic of China*

Yinfu Liu − *Interdisciplinary Materials Research Center, College of Materials Science and Engineering, Tongji University, Shanghai 201804, People's Republic of China*

Lina Shang − *Interdisciplinary Materials Research Center, College of Materials Science and Engineering, Tongji University, Shanghai 201804, People's Republic of China*

Yangfan Wu − *CAS Key Laboratory of Standardization and Measurement for Nanotechnology, CAS Center for Excellence in Nanoscience, National Center for Nanoscience and Technology, Beijing 100190, People's Republic of China; School of Future Technology, University of Chinese Academy of Sciences, Beijing 100049, People's Republic of China*

Hui-Jun Jiang − *Hefei National Laboratory for Physical Sciences at the Microscale & Department of Chemical Physics, iChEM, University of Science and Technology of China, Hefei, Anhui 230026, People's Republic of China;* orcid.org/0000-0001-7243-5431

Complete contact information is available at: https://pubs.acs.org/10.1021/acsnano.1c07842

Author Contributions

‡D.L. and L.S. contributed equally to this work.

Author Contributions

All authors have given approval to the final version of the manuscript.

Notes

The authors declare no competing financial interest.

ACKNOWLEDGMENTS

The authors acknowledge the financial support from the National Natural Science Foundation of China (21790351, 21790353, 21972032, 21721002, 21425310, 22072086), the Ministry of Science and Technology of China (Grant Nos. 2017YFA0205000 and 2016YFA0200700), the Strategic Priority Research Program of Chinese Academy of Sciences (XDB36000000), and the Scientific Instrument Developing Project of the Chinese Academy of Sciences (Grant No. GJJSTD20200005).

REFERENCES

(1) Pasteur, L. Recherches Sur Les Relations Qui Peuvent Exister Entre La Forme Cristalline: La Composition Chimique Et Les Sens De La Polarisation Rotatoire. *Ann. Chim. Phys.* **1848**, *24*, 442–459.

(2) Geiger, Y.; Achard, T.; Maisse-François, A.; Bellemin-Laponnaz, S. Hyperpositive Nonlinear Effects in Asymmetric Catalysis. *Nat. Catal.* **2020**, *3*, 422–426.

(3) Reyes, R. L.; Sato, M.; Iwai, T.; Suzuki, K.; Maeda, S.; Sawamura, M. Asymmetric Remote C–H Borylation of Aliphatic Amides and Esters with a Modular Iridium Catalyst. *Science* **2020**, *369*, 970–974.

(4) Shimomura, K.; Ikai, T.; Kanoh, S.; Yashima, E.; Maeda, K. Switchable Enantioseparation Based on Macromolecular Memory of a Helical Polyacetylene in the Solid State. *Nat. Chem.* **2014**, *6*, 429–434.

(5) Hou, K.; Zhao, J.; Wang, H.; Li, B.; Li, K.; Shi, X.; Wan, K.; Ai, J.; Lv, J.; Wang, D.; Huang, Q.; Wang, H.; Cao, Q.; Liu, S.; Tang, Z. Chiral Gold Nanoparticles Enantioselectively Rescue Memory Deficits in a Mouse Model of Alzheimer's Disease. *Nat. Commun.* **2020**, *11*, No. eabd5290.

(6) Lu, Y.; Swisher, J. H.; Meyer, T. Y.; Coates, G. W. Chirality-Directed Regioselectivity: An Approach for the Synthesis of

Alternating Poly(lactic-Co-Glycolic Acid). *J. Am. Chem. Soc.* **2021**, *143*, 4119−4124.
(7) Saha, D.; Kharbanda, A.; Yan, W.; Lakkaniga, N. R.; Frett, B.; Lii, H. Y. The Exploration of Chirality for Improved Druggability within the Human Kinome. *J. Med. Chem.* **2020**, *63*, 441−469.
(8) Savile, C. K.; Janey, J. M.; Mundorff, E. C.; Moore, J. C.; Tarn, S.; Jarvis, W. R.; Colbeck, J. C.; Krebber, A.; Fleitz, F. J.; Brands, J.; Devine, P. N.; Huisman, G. W.; Hughes, G. J. Biocatalytic Asymmetric Synthesis of Chiral Amines from Ketones Applied to Sitagliptin Manufacture. *Science* **2010**, *329*, 305−309.
(9) Waldeck, B. Three-Dimensional Pharmacology, a Subject Ranging from Ignorance to Overstatements. *Pharmacol. Toxicol.* **2003**, *93*, 203−210.
(10) Xi, S.; Dong, J.; Chen, H.; Dong, Q.; Yang, J.; Tan, Q.; Zhang, C.; Lan, Y.; Zhang, M. Lewis Acid−Catalyzed Domino Generation/[2,3]-Sigmatropic Earrangement of Ammonium Ylides to Access Chiral Azabicycles. *Sci. Adv.* **2021**, *7*, No. eabd5290.
(11) Feng, Y.; Wang, M.; Zhang, D.; Yang, J.; Li, Y. Chirality Pure Carbon Nanotubes: Growth, Sorting, and Characterization. *Chem. Rev.* **2020**, *120*, 2693−2758.
(12) Hou, K.; Ali, W.; Lv, J.; Guo, J.; Shi, L.; Han, B.; Wang, X.; Tang, Z. Optically Active Inverse Opal Photonic Crystals. *J. Am. Chem. Soc.* **2018**, *140*, 16446−16449.
(13) Li, J.; Neupert, T.; Wang, Z.; MacDonald, A. H.; Yazdani, A.; Bernevig, B. A. Two-Dimensional Chiral Topological Superconductivity in Shiba Lattices. *Nat. Commun.* **2016**, *7*, 12297.
(14) Shopsowitz, K. E.; Qi, H.; Hamad, W. Y.; Maclachlan, M. J. Free-Standing Mesoporous Silica Films with Tunable Chiral Nematic Structures. *Nature* **2010**, *468*, 422−425.
(15) Breslow, R.; Levine, M. S. Amplification of Enantiomeric Concentrations under Credible Prebiotic Conditions. *Proc. Natl. Acad. Sci. U. S. A.* **2006**, *103*, 12979−12980.
(16) Ernst, K. H. Molecular Chirality at Surfaces. *Phys. Status Solidi B* **2012**, *249*, 2057−2088.
(17) Tamura, K.; Schimmel, P. R. Chiral-Selective Aminoacylation of an RNA Minihelix: Mechanistic Features and Chiral Suppression. *Proc. Natl. Acad. Sci. U. S. A.* **2006**, *103*, 13750−13752.
(18) Laage, D.; Elsaesser, T.; Hynes, J. T. Water Dynamics in the Hydration Shells of Biomolecules. *Chem. Rev.* **2017**, *117*, 10694−10725.
(19) Xie, L.; Jiang, H. J.; Li, D. L.; Liu, M. X.; Ding, Y. Q.; Liu, Y. F.; Li, X.; Li, X. C.; zhang, H. M.; Hou, Z. H.; Luo, Y.; Chi, L. F.; Qiu, X. H.; Xu, W. Selectively Scissoring Hydrogen-Bonded Cytosine Dimer Structures Catalyzed by Water Molecules. *ACS Nano* **2020**, *14*, 10680−10687.
(20) Kawasaki, T.; Hakoda, Y.; Mineki, H.; Suzuki, K.; Soai, K. Generation of Absolute Controlled Crystal Chirality by the Removal of Crystal Water from Achiral Crystal of Nucleobase Cytosine. *J. Am. Chem. Soc.* **2010**, *132*, 2874−2875.
(21) Song, C. E.; Park, S. J.; Hwang, I.; Jung, M. J.; Shim, S. Y.; Bae, H. Y.; Jung, J. Y. Hydrophobic Chirality Amplification in Confined Water Cages. *Nat. Commun.* **2019**, *10*, 851.
(22) Johnson, R. S.; Yamazaki, T.; Kovalenko, A.; Fenniri, H. Molecular Basis for Water-Promoted Supramolecular Chirality Inversion in Helical Rosette Nanotubes. *J. Am. Chem. Soc.* **2007**, *129*, 5735−5743.
(23) Chen, T.; Wang, D.; Wan, L. J. Two-Dimensional Chiral Molecular Assembly on Solid Surfaces: Formation and Regulation. *Natl. Sci. Rev.* **2015**, *2*, 83−94.
(24) Chen, T.; Yang, W. H.; Wang, D.; Wan, L. J. Globally Homochiral Assembly of Two-Dimensional Molecular Networks Triggered by Co-Absorbers. *Nat. Commun.* **2013**, *4*, 1389.
(25) Mairena, A.; Zoppi, L.; Seibel, J.; Trster, A. F.; Ernst, K. H. Heterochiral to Homochiral Transition in Pentahelicene 2D Crystallization Induced by Second-Layer Nucleation. *ACS Nano* **2017**, *11*, 865−871.
(26) Parschau, M.; Ernst, K. Disappearing Enantiomorphs: Single Handedness in Racemate Crystals. *Angew. Chem., Int. Ed.* **2015**, *54*, 14422−14426.
(27) Stetsovych, O.; Svec, M.; Vacek, J.; Chocholousová, J. V.; Jancarik, A.; Rybácek, J.; Kosmider, K.; Stará, I. G.; Jelínek, P.; Stary, I. From Helical to Planar Chirality by On-Surface Chemistry. *Nat. Chem.* **2017**, *9*, 213−218.
(28) Kühnle, A.; Linderoth, T. R.; Hammer, B.; Besenbacher, F. Chiral Recognition in Dimerization of Adsorbed Cysteine Observed by Scanning Tunnelling Microscopy. *Nature* **2002**, *415*, 891−893.
(29) Ernst, K. H.; Baumann, S.; Lutz, C. P.; Seibel, J.; Zoppi, L.; Heinrich, A. J. Pasteur's Experiment Performed at the Nanoscale: Manual Separation of Chiral Molecules, One by One. *Nano Lett.* **2015**, *15*, 5388−5392.
(30) Martin, J. D.; Ahles, S.; Mollenhauer, D.; Wegner, H. A.; Schirmeisen, A.; Ebeling, D. Bond-Level Imaging of the 3D Conformation of Adsorbed Organic Molecules Using Atomic Force Microscopy with Simultaneous Tunneling Feedback. *Phys. Rev. Lett.* **2019**, *122*, 196101.1−196101.6.
(31) Besenbacher, F. Scanning Tunnelling Microscopy Studies of Metal Surfaces. *Rep. Prog. Phys.* **1996**, *59*, 1737−1802.
(32) Laegsgaard, E.; Österlund, L.; Thostrup, P.; Rasmussen, P.; Stensgaard, I.; Besenbacher, F. A High-Pressure Scanning Tunneling Microscope. *Rev. Sci. Instrum.* **2001**, *72*, 3537−3542.
(33) Ji, C.; Jing, G.; Meng, X.; Peng, J.; Wang, E. G. An Unconventional Bilayer Ice Structure on a NaCl(001) Film. *Nat. Commun.* **2014**, *5*, 4056.
(34) Kresse, G.; Furthmuller, J. Efficient Iterative Schemes for *ab Initio* Total-Energy Calculations Using a Plane-Wave Basis Set. *Phys. Rev. B: Condens. Matter Mater. Phys.* **1996**, *54*, 11169−11186.
(35) Kresse, G.; Hafner, J. *Ab Initio* Molecular Dynamics for Open-Shell Transition Metals. *Phys. Rev. B: Condens. Matter Mater. Phys.* **1993**, *48*, 13115−13118.
(36) Perdew, J.; Burke, K.; Ernzerhof, M. Generalized Gradient Approximation Made Simple. *Phys. Rev. Lett.* **1996**, *77*, 3865−3868.
(37) Blochl, P. E. Projector Augmented-Wave Method. *Phys. Rev. B: Condens. Matter Mater. Phys.* **1994**, *50*, 17953−17979.
(38) Kresse, G.; Joubert, D. From Ultrasoft Pseudopotentials to the Projector Augmented-Wave Method. *Phys. Rev. B: Condens. Matter Mater. Phys.* **1999**, *59*, 1758−1775.
(39) Grimme, S.; Antony, J.; Ehrlich, S.; Krieg, H. A Consistent and Accurate *ab Initio* Parametrization of Density Functional Dispersion Correction (DFT-D) for the 94 Elements H-Pu. *J. Chem. Phys.* **2010**, *132*, 154104.
(40) Frisch, M. J.; Trucks, G. W.; Schlegel, H. B.; Scuseria, G. E.; Robb, M. A.; Cheeseman, J. R.; Scalmani, G.; Barone, V.; Petersson, G. A.; Nakatsuji, H.; Li, X.; Caricato, M.; Marenich, A. V.; Bloino, J.; Janesko, B. G.; Gomperts, R.; Mennucci, B.; Hratchian, H. P.; Ortiz, J. V.; Izmaylov, A. F.; et al. *Gaussian 09* Rev. A.02; Gaussian, Inc.: Wallingford, CT, 2016.
(41) Tian, L.; Chen, F. Multiwfn: A Multifunctional Wavefunction Analyzer. *J. Comput. Chem.* **2012**, *33*, 580−592.
(42) Hapala, P.; Temirov, R.; Tautz, F. S.; Jelínek, P. Origin of High-Resolution IETS-STM Images of Organic Molecules with Functionalized Tips. *Phys. Rev. Lett.* **2014**, *113*, 226101.

https://doi.org/10.1021/acsnano.1c07842
ACS Nano XXXX, XXX, XXX−XXX